Proceedings Paper:

Perera, AGU, Lao, Y-F, Li, LH et al. (2015) Tunable hot-carrier photodetectors for terahertz frequency operation. In: Proceedings of a meeting held 16-18 March 2015, Cambridge, Massachusetts, USA. 26th International Symposium on Space Terahertz Technology, 16-18 Mar 2015, Cambridge, MA, USA. International Symposium on Space Terahertz Technology, 129 - 132. ISBN: 9781510809338.

Tunable hot-carrier photodetectors for terahertz frequency operation

A. G. Unil Perera[1,*], Yan-Feng Lao[1], L. H. Li[2], S. P. Khanna[2], and E. H. Linfield[2]
[1]*Department of Physics and Astronomy, Georgia State University, Atlanta, GA 30303, USA*
[2]*School of Electronic and Electrical Engineering, University of Leeds, Leeds LS2 9JT, United Kingdom*
*Contact: uperera@gsu.edu, phone +1-404-413-6037

Abstract—**The cut-off wavelength limit (λ_c) in traditional photodetectors is determined by the activation energy (Δ) of the semiconductor structure, and is given by the relationship: λ_c = hc/Δ. This empirical spectral rule has dominated device design for many years, and was thought to limit intrinsically the long wavelength response of a photodetector. Recently, however, we have demonstrated a new, long wavelength photodetection principle using a hot-cold carrier energy transfer mechanism. Hot carriers injected into a semiconductor structure interact with cold carriers and excite them to higher energy states. This has enabled a very long-wavelength infrared response up to 55 µm to be achieved, which is tunable by varying the degree of hot-hole carrier injection.**

I. Introduction

The typical operating principle of a heterojunction photodetector is photoexcitation of carriers in the absorber (or emitter), and their escape over the barrier by an internal photoemission process occurring at the emitter-barrier interface.[1] The ability for carriers to escape is characterized by an internal work function (Δ), which is defined as the energy difference between the Fermi level of the absorber and the band edge of the barrier. This photoemission threshold energy is traditionally thought to limit the photoresponse threshold. However, modifying the energy distribution of carriers, for example by introducing hot-cold carrier interactions, leads to a change in this threshold response.

Hot-carrier dynamics have been the subject of many studies in semiconductor physics and devices,[2-4] and there has been increasing interest in using hot-carrier driven effects for photodetection.[5-8] Here, we demonstrate an extension of the spectral threshold into the very-long wavelength infrared (VLWIR) range. A *p*-type GaAs/AGaAs heterojunction detector (Fig. 1) with Δ = 0.32 eV (or 3.9 µm in wavelength) showed a response up to 103 µm. A clear advantage of our approach is to minimize the detector noise since the hot-carrier concept allows separating the photoemission threshold from determining the threshold response.

II. Device structure

Semiconductor heterostructures based on *p*-type GaAs/$Al_xGa_{1-x}As$ were used to study hot-carrier detection. As shown in Fig. 1 (a), they consist of three *p*-type GaAs regions (doped at p = 1 × 10^{19} cm^{-3}), i.e., an injector, absorber and collector, for which the VB alignment is schematically plotted in Figs. 1 (b). The injector provides a hot-hole reservoir upon photoexcitation. Holes surmounting the barrier are “hot” because of their excess energies relative to the band edge of the absorber.

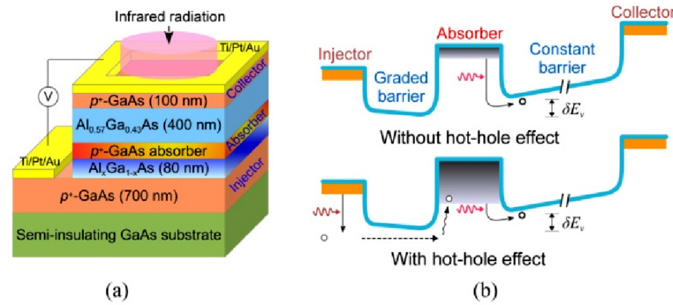

Fig. 1 (a) Schematic of the *p*-type GaAs/$Al_xGa_{1-x}As$ hot-hole photodetector structure. (b) Schematic valence-band diagrams (including band bending) under negative bias (positive polarity applied on the injector), with a comparison of hole photoexcitation and emission without (top) and with (bottom) hot-cold hole energy transfer. δE_v is the offset between the barriers below and above the *p*-GaAs absorber

III. Results and discussion

The detector dark current measured experimentally [Fig. 2 (a)] was fitted well by a thermionic emission model [9] using the activation energies arising from the design .

The photoresponse shown in Fig. 2 (b) was measured at 5.3 K. The most striking fact is that, a very long-wavelength infrared (VLWIR) response is seen up to 55 µm, whilst the conventional limit is only 3.9 µm (shaded region) according to the value of Δ of the absorber/constant barrier junction (i.e., 0.32 eV). Fig. 2 (c) shows the bias dependent spectral weight.[10] The agreement between λ_c and Δ in terms of the spectral rule λ_c = hc/Δ is typically found to be good in a variety of detectors, and has been used as a guideline to tune spectral response through varying Δ, and to determine band offsets. However, the observed VLWIR response threshold in this case contradicts the value of Δ given by spectral rule.

In general, an observed VLWIR response could be due to a bolometric effect, or an impurity-band/free-hole carrier based response, both of which are associated with the absorber. Possible optical transitions contributing to photon absorption by the *p*-type GaAs absorber in the infrared range include impurity band-to-valence band transitions, and intra-/inter-valence band transitions, both of which are free-carrier type effects. We have measured another sample which contains the

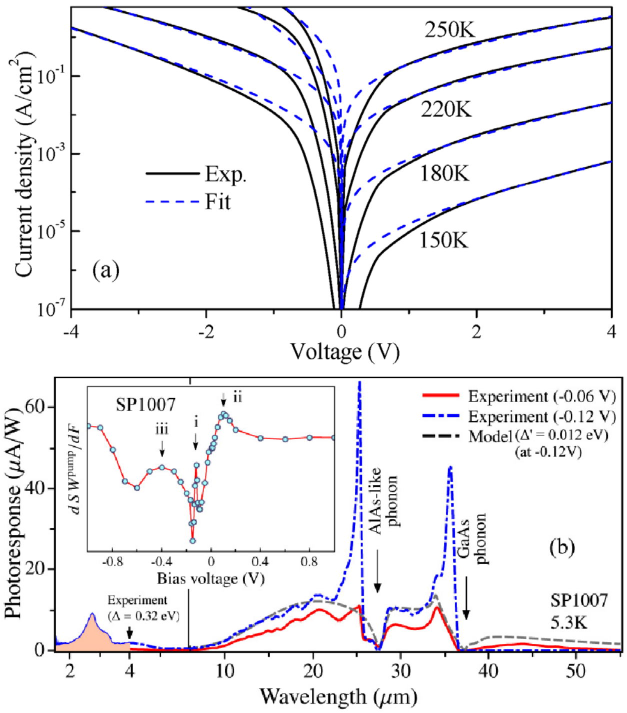

Fig. 2 (a) Experimental and theoretical dark current-voltage (I-V) characteristic for sampe SP1007; the fittings are based on the thermionic emission model, with active energies of 032 eV and 0.40 eV for reverse and forward biases, respectively. (b) Experimental photoresponse at 5.3 K, and the escape-cone model (dashed line) fit, with a reduced threshold energy (Δ') of 0.012 eV (103 µm in wavelength). The marked arrows are associated with GaAs and AlAs-like phonons. Inset: Differential spectral weight (*SW*) (Eq. 3) as a function of bias, showing peaks i, ii and iii. SW^{pump} is calculated using λ_{max} = 2.95 µm (i.e., 0.42 eV, the maximum of the graded barrier).

same GaAs absorber, but consisting of symmetrical and constant barriers above and below the absorber. The fact that this sample does not show the VLWIR response allows us to exclude these two mechanisms as a cause of the VLWIR response. In addition, the bolometric response, proportional to the temperature variation of the absorber upon photon absorption and its corresponding resistance change, monotonically increases with increasing bias. This effect contrasts with the strongly non-monotonically bias-dependent VLWIR response observed. As seen in Fig. 2 (b), the observed VLWIR response agrees well with a fitting value Δ = 0.012 eV (escape-cone model), although the design and Arrhenius plot gives Δ = 0.32 eV. Features associated with GaAs and AlAs-like phonons are, however, also well explained by the escape-cone model with a value of 0.012 eV (103 µm).

The hot-cold carrier energy transfer mechanism is in part supported by differential photocurrent measurements. The short-wavelength portion of light from either a Fourier transform infrared (FTIR) spectrometer, or from an external optical excitation source (denoted as the "pump") are an essential requirement as they generate the photoexcited hot holes that are needed to observe the VLWIR response. The pump-excited holes with energies above all of the device barriers can be described by a three-dimensional drift model,[11]

$$I_{ph}^{pu} = e \cdot v(F) \int_{\Delta}^{+\infty} N(\varepsilon) d\,\varepsilon \qquad (1)$$

where dI_{ph}^{pu} is the pump current. and $N(\varepsilon)$ is the concentration of holes with energy ε. The electric field F is evaluated across the barrier regions. The drift velocity $v(F)$ is associated with an empirical fitting parameter - the mobility, which is dependent upon both the doped GaAs absorber and undoped AlGaAs barriers. Despite its simplicity, Eq. 1 accounts for the current-voltage characteristics reasonably well in most devices. Taking the derivative of I_{ph} with respect to F gives

$$\frac{dI_{ph}^{pu}}{dF} = e \cdot \frac{dv(F)}{dF} \int_{\Delta}^{+\infty} N(\varepsilon) d\,\varepsilon - e \cdot v(F) \frac{d\Delta}{dF} N(\Delta) \qquad (2)$$

in which dI_{ph}^{pu}/dF is mainly determined by the image-force barrier lowering[1] and tilting of the graded barrier by applied bias. In the high-field region, the first term of Eq. 2 vanishes since $v(F)$ approaches a constant saturation velocity. The energy distribution of holes is thus proportional to the differential I_{ph}^{pu}, which consists of photocarriers with different energies. I_{ph}^{pu} can be evaluated as being proportional to the spectral weight (SW) of the response, defined as

$$SW \propto \int_{\lambda_{min}}^{\lambda_{max}} R(\lambda) d\lambda \qquad (3)$$

where $R(\lambda)$ is the spectral responsivity. As seen in the inset of Fig. 2 (b), the differential *SW* displays three distribution peaks at -0.12, -0.40 and 0.10 V, which were confirmed by photocurrent-voltage characteristics measured using a different optical excitation source.

In terms of hot-carrier spectroscopy,[12] the occurrence of distribution peaks is a sign of a hot-cold carrier interaction which leads to the excitation of cold carriers into higher energy states. With increasing negative bias, the slope of the graded barrier is reduced (towards a horizontal shape). An increase in the injection of hot holes and enhanced hot-cold interactions is then expected, which consequently leads to an increase in cold holes occupying higher energy states. This explains the distribution peak at -0.12 V. When the bias is further increased, the electric field is distributed uniformly throughout the structure. The lowering of the constant barrier by the image-force effect will facilitate the escape of higher-energy cold holes over the barrier, which leads to another distribution peak at higher negative bias (-0.40 V). At such high biases, the hot-hole related current is also high, and this overwhelms the VLWIR radiation caused photocurrent.

Observing a positive-bias hole distribution peak (0.10 V) is uncommon. A possible reason is the non-linear increase of photocurrent with bias due to the asymmetric band alignment. However, applying a negative bias leads to the optimum VLWIR response, which is much stronger than that observed under positive bias. The three distribution peaks depend on the structural details of the device, such as the graded barrier composition and the barrier offset. As such, an ability to control these parameters should lead to tunability of the hot-hole photodetection.

The occurrence of the VLWIR response due to a hot-cold carrier interaction means that one can tune the degree of hot-hole injection to control this response. The experimental setup shown in Fig. 3 was used to demonstrate the tuning of the VLWIR response. A λ_{CO} =4.5 µm (corresponding to 0.28 eV) long-pass filter is used to prevent the high-energy (> 0.28 eV) photons (from a spectrometer) from being incident onto the sample. The generation of hot holes is instead enabled using an external high-energy light source. For comparison, the original wavelength-extended response (without using filter

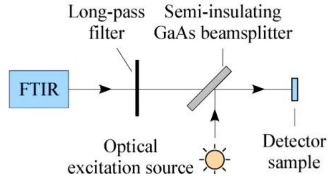

Fig. 3 Experimental apparatus, where the double-side polished semi-insulating GaAs wafer acts as a beamsplitter.

and external optical excitation source) is shown in Fig. 4. The photocurrent, represented by the spectral weight of the response, at different levels is shown in Fig. 5 (a). Fig. 5 (b) shows the excitation power spectra. The variation of the VLWIR response (at -0.1 V) with the excitation power is plotted in Figs. 4 (c), indicating that the VLWIR response is enabled by increasing the excitation intensity, demonstrating a response tunability through varying the degree of hot-hole injection.

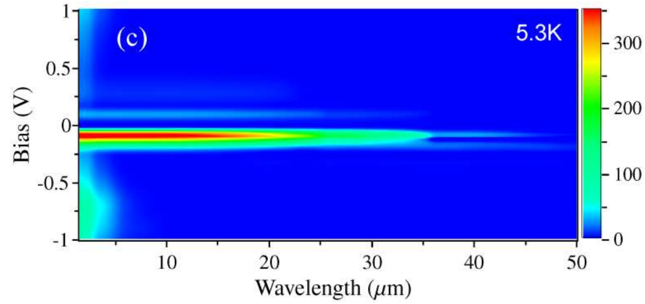

Fig. 4 Variation of spectral weight with bias and wavelength. The measurement was carried without using filters and external excitation source.

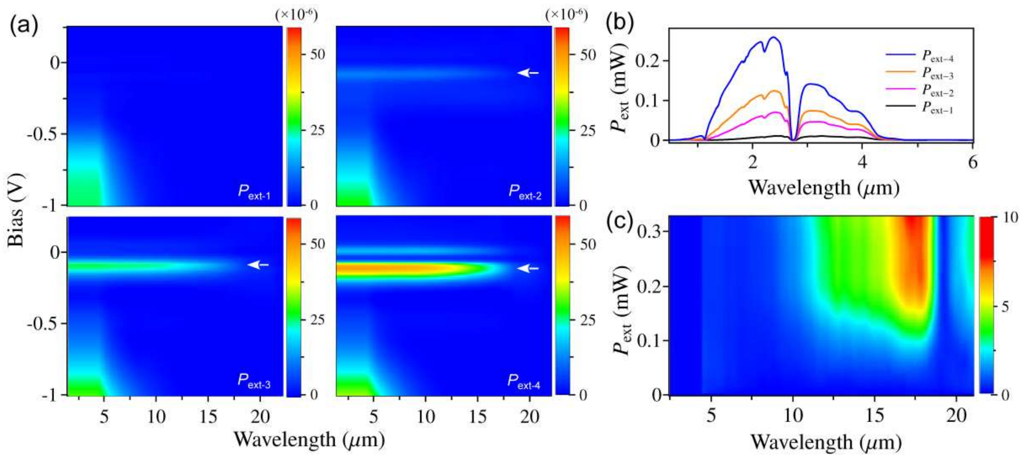

Fig. 5 (a) Spectral weights of response obtained using different intensities of optical excitation source (P_{ext-1} - P_{ext-4}). The left image in the first panel was obtained using P_{ext-1}, which is very similar to the case where the external optical source is fully blocked. (b) Power spectra of the excitation optical source (incident on the sample with an active area of 260 × 260 μm^2). A quartz glass filter is used to enable spectra up to 4.8 μm which ensures the excitation optical source is only used to excite hot holes. (c) The dependence of the VLWIR response (at -0.1 V) on the excitation power.

As an alternative to the bulk *p*-type doped absorber used in this work, a nano-structure, for example a quantum well or dot, could be used in order to enhance the hot-carrier effect owing to the extended carrier lifetime resulting from confinement of the carriers. Also, surface plasmon and cavity resonances could be used to enhance further the optical electric field and hence the absorption. These would be expected to contribute to a significant increase in responsivity, as well as an elevated operating temperature.

IV. Conclusions

We have demonstrated an internal photoemission detector with response up to 55 μm, which is tunable by varying the degree of hot-hole injection. This has been achieved using a GaAs/AlGaAs device with Δ = 0.32 eV (equivalent to a 3.9 μm cut-off wavelength).

Acknowledgment

This work was supported in part by the US Army Research Office (grant no. W911NF-12-2-0035), monitored by William W. Clark, and in part by the US National Science Foundation (grant no. ECCS-1232184, monitored by Mahmoud Fallahi). We also acknowledge support from the ERC grant 'TOSCA', and EPSRC (UK).

References

1. Y.-F. Lao and A. G. U. Perera, Phys. Rev. B **86** (19), 195315 (2012).
2. S. Winnerl, M. Orlita, P. Plochocka, P. Kossacki, M. Potemski, T. Winzer, E. Malic, A. Knorr, M. Sprinkle, C. Berger, W. A. de Heer, H. Schneider and M. Helm, Phys. Rev. Lett. **107** (23), 237401 (2011).
3. F. Rossi and T. Kuhn, Reviews of Modern Physics **74** (3), 895-950 (2002).
4. Y. Rosenwaks, M. C. Hanna, D. H. Levi, D. M. Szmyd, R. K. Ahrenkiel and A. J. Nozik, Phys. Rev. B **48** (19), 14675-14678 (1993).
5. M. Freitag, T. Low, F. Xia and P. Avouris, Nat Photon **7** (1), 53-59 (2013).
6. N. M. Gabor, J. C. W. Song, Q. Ma, N. L. Nair, T. Taychatanapat, K. Watanabe, T. Taniguchi, L. S. Levitov and P. Jarillo-Herrero, Science **334** (6056), 648-652 (2011).
7. Z. Sun, Z. Liu, J. Li, G.-a. Tai, S.-P. Lau and F. Yan, Advanced Materials **24** (43), 5878-5883 (2012).
8. J. Yan, M. H. Kim, J. A. Elle, A. B. Sushkov, G. S. Jenkins, H. M. Milchberg, M. S. Fuhrer and H. D. Drew, Nat Nano **7** (7), 472-478 (2012).
9. D. G. Esaev, M. B. M. Rinzan, S. G. Matsik and A. G. U. Perera, J. Appl. Phys. **96** (8), 4588-4597 (2004).
10. Y.-F. Lao, A. G. U. Perera, L. H. Li, S. P. Khanna, E. H. Linfield and H. C. Liu, Nat Photon **8** (5), 412-418 (2014).
11. H. Schneider and H. C. Liu, *Quantum well infrared photodetectors : physics and applications*. (Springer, New York, 2007).
12. A. F. J. Levi, J. R. Hayes, P. M. Platzman and W. Wiegmann, Phys. Rev. Lett. **55** (19), 2071-2073 (1985).